

SEA WAVE PATTERN EVALUATION

Part 3 Report: Near-Field Waves

E.O. Tuck, D.C. Scullen and L. Lazauskas

Applied Mathematics Department
The University of Adelaide

January 31, 2000

Abstract

This is the third report in a series describing a computer program *SWPE* which is intended eventually to provide a full description of the wave elevation and flow field created by a surface-piercing or submerged body moving steadily forward in still water of constant depth. The first two reports (produced at The University of Adelaide) provided results in the so-called far field, notionally several shiplengths aft of the body. In the present report this is generalised to provide wave elevations in infinite depth of water at any point near or far from the body.

The front cover of this report is a contour plot of wave elevations predicted by *SWPE* for a DDG51 destroyer model travelling at a Froude number of 0.4136, equivalent to 30 knots full-scale speed.

1 Introduction

Near-field ship-wave computation is a very difficult task. Even if linearisation is allowed as is assumed here, so that Michell's thin-ship theory can be used, the task still involves at least one order of magnitude greater difficulty than that of computing waves in the far field. Notably, it involves one extra numerical integration. In the first sections to follow of this report, we give the full thin-ship theory on which our method is based.

Results are then presented for a particular vessel, which is a model for a proposed US Navy DDG51 ship represented by David Taylor Model Basin (DTMB) Model 5415, having a bow bulb and a transom stern. This model was used as one of the test hulls for the 1991 "Wake-Off" evaluation at DTMB, where a number of then-current computer programs were assessed for their ability to agree with towing tank measurements of the near-field wave patterns. In summary, we demonstrate here that the present SWPE code is able to do at least as well as any of those codes.

One important factor included here as an option is the effect of viscosity on the wave pattern. Although SWPE produces good results on a purely inviscid basis, even better agreement with some aspects of the experimental data is obtained if damping of waves is allowed according to a standard formula involving a kinematic viscosity coefficient which takes values between 0.001 and $0.01\text{m}^2\text{s}^{-1}$, which is a sensible range for an eddy viscosity in oceanographic contexts.

2 Formulation via the Michell potential

The velocity potential of a unit Havelock source ([3] p. 28, [17] p. 484, [8], [16]) located at $(x, y, z) = (0, 0, \zeta)$, or "free-surface Green's function", is given by the double integral

$$G(x, y, z; \zeta) = -\frac{1}{4\pi^2} \Re \int_{-\pi/2}^{\pi/2} d\theta \int_0^\infty dk e^{-ik(x \cos \theta + y \sin \theta)} \left[e^{-k|z-\zeta|} - \frac{k + k_0 \sec^2 \theta}{k - k_0 \sec^2 \theta} e^{k(z+\zeta)} \right] \quad (1)$$

where the path of k -integration passes *above* the pole at $k = k_0 \sec^2 \theta$, with $k_0 = g/U^2$. The first term inside the square bracket of (1) contributes the potential of

an ordinary infinite-fluid Rankine source, since

$$-\frac{1}{4\pi^2} \Re \int_{-\pi/2}^{\pi/2} d\theta \int_0^\infty dk e^{-ik(x \cos \theta + y \sin \theta) - k|z - \zeta|} = -\frac{1}{4\pi \sqrt{x^2 + y^2 + (z - \zeta)^2}}. \quad (2)$$

The second term inside the square bracket of (1) is the correction for the free surface, and it is easy to verify the Kelvin free-surface condition $G_{xx} + k_0 G_z = 0$ on $z = 0$.

Now let us distribute Havelock sources over a region R of the plane $y = 0$, with strength $m(\xi, \zeta)$ per unit area at the point $(\xi, 0, \zeta)$. Thus

$$\phi(x, y, z) = \iint_R d\xi d\zeta m(\xi, \zeta) G(x - \xi, y, z; \zeta). \quad (3)$$

For the present report we assume that $z \geq \zeta$ throughout R , which is certainly true on the free surface $z = 0$. Then we find that

$$\begin{aligned} \phi(x, y, z) = & -\frac{1}{4\pi^2} \Re \int_{-\pi/2}^{\pi/2} d\theta \int_0^\infty dk e^{-ik(x \cos \theta + y \sin \theta)} \\ & \left[e^{-kz} - \frac{k + k_0 \sec^2 \theta}{k - k_0 \sec^2 \theta} e^{kz} \right] \iint_R d\xi d\zeta m(\xi, \zeta) e^{ik\xi \cos \theta + k\zeta} \end{aligned} \quad (4)$$

Now Michell [7] says that for a monohull thin ship with offsets $y = \pm Y(x, z)$, the disturbance velocity potential is given by the above expression, where the source strength is proportional to the longitudinal slope, namely

$$m(\xi, \zeta) = 2UY_\xi(\xi, \zeta). \quad (5)$$

Substituting into (4) and integrating by parts with respect to ξ , we get

$$\begin{aligned} \phi(x, y, z) = & \frac{U}{2\pi^2} \Re i \int_{-\pi/2}^{\pi/2} d\theta \int_0^\infty dk e^{-ik(x \cos \theta + y \sin \theta)} \\ & k_1 \left[e^{-kz} - \frac{k + k_0 \sec^2 \theta}{k - k_0 \sec^2 \theta} e^{kz} \right] (P + iQ) \end{aligned} \quad (6)$$

where

$$P + iQ = -\frac{1}{ik_1} \iint_R d\xi d\zeta Y_\xi(\xi, \zeta) e^{ik_1 \xi + k\zeta} \quad (7)$$

$$= \iint_R d\xi d\zeta Y(\xi, \zeta) e^{ik_1 \xi + k\zeta} - \frac{1}{ik_1} e^{ik_1 \xi_S} \int Y(\xi_S, \zeta) e^{k\zeta} d\zeta \quad (8)$$

with $k_1 = k \cos \theta$ as the x -wise wave number.

The formula (7) for $P + iQ$ is valid for any bow or stern ends, whereas the formula (8) has been integrated by parts, assuming a bow with zero offsets but a stern $\xi = \xi_S$ with a transom having non-zero offsets $y = \pm Y(\xi_S, \zeta)$. If there is no transom, then the second term of (8) vanishes, and we have simply $P = \int R(\xi) \cos(k_1 \xi) d\xi$, with a similar formula for Q involving the sine, and $R(\xi) = \int Y(\xi, \zeta) \exp(k\zeta) d\zeta$. If there is a transom, this P is replaced by $P - R(\xi_S) \sin(k_1 \xi_S) / k_1$ and Q is replaced by $Q + R(\xi_S) \cos(k_1 \xi_S) / k_1$.

The linearised wave elevation $z = Z(x, y)$ is then given by

$$Z(x, y) = -\frac{U}{g} \phi_x(x, y, 0) \quad (9)$$

$$= \frac{1}{\pi^2} \Re \int_{-\pi/2}^{\pi/2} d\theta \int_0^\infty dk \frac{k^2}{k - k_0 \sec^2 \theta} (P + iQ) e^{-ik(x \cos \theta + y \sin \theta)}. \quad (10)$$

2.1 Separation into components

Remember that the path of k -integration presently goes *above* the pole. This was in order to ensure that waves lie behind the ship; more to the point, that there are no waves ahead of the ship. In particular, if we were to go *below* the pole, this would reverse the direction and put waves ahead of the ship, not behind it. To emphasise this fact, suppose we define Z^- as the (incorrect) solution where the path goes below the pole, to distinguish it from our desired solution Z .

Now let us define $Z^0 = Z - Z^-$. Then by the residue theorem, the k -integral for Z^0 is just $-2\pi i$ times the residue of Z at the pole. Thus

$$Z^0(x, y) = -\frac{2k_0^2}{\pi} \Re i \int_{-\pi/2}^{\pi/2} d\theta \sec^4 \theta (P + iQ) e^{-ik_0 \sec^2 \theta (x \cos \theta + y \sin \theta)} \quad (11)$$

with $k = k_0 \sec^2 \theta$ in the formula (7) for $P + iQ$.

Since Z^- has no waves behind the body, if we let $x \rightarrow +\infty$ then $Z^- \rightarrow 0$, so $Z^0 \rightarrow Z$. That is, Z^0 is precisely the usual far-field formula for the wave elevation. This formula was used in SWPE2.0 and is given in the Part 1 report [13].

It is convenient also to define a Cauchy principal-value integral which is just the average of Z and Z^- , i.e.

$$Z^C = \frac{1}{2}[Z + Z^-] = Z - \frac{1}{2}Z^0. \quad (12)$$

Rearranging, we see that we can compute the full Michell elevation function Z as

$$Z = Z^C + \frac{1}{2}Z^0. \quad (13)$$

If we have a computer program for the Cauchy principal-value Z^C and for the far field Z^0 , we can therefore easily compute the full wave field Z .

If we then want the purely local field, Z^L which (for an origin located between bow and stern) has no waves either ahead of the bow or behind the stern, we can define it to be $Z^L = Z$ if $x < 0$, and $Z^L = Z^- = Z - Z^0$ if $x > 0$. Rearranging, we have

$$Z = \begin{cases} Z^L, & x < 0 \\ Z^L + Z^0, & x > 0 \end{cases} \quad (14)$$

$$= Z^L + Z^F \quad (15)$$

where Z^F is the far-field contribution defined by $Z^F = Z^0H(x)$ and $H(x)$ is the Heaviside unit step function. Thus the total wave field can be written as the sum $Z = Z^L + Z^F$ of a local and far-field contribution. Also, in terms of the Cauchy principal-value integral, the local-field contribution is

$$Z^L = Z^C - \frac{1}{2}Z^0\text{sgn}x. \quad (16)$$

3 Formulation via direct convolution

The above is the way to compute waves in the spirit of Michell [7], and of SWPE2 . 0. Namely, spectrum functions $P + iQ$ of wavenumber are first computed by integration of offset data over the centreplane, then integrands involving these functions are integrated with respect to wavenumber and direction.

However, another possibility is somewhat more direct, as follows. Suppose we have available (by numerical integration with respect to wavenumber and direction or otherwise) computer code for the Green's function G itself, as defined by (1). Then according to a combination of (3) and (5),

$$\phi(x, y, z) = 2U \iint_R Y_\xi(\xi, \zeta) G(x - \xi, y, z; \zeta) d\xi d\zeta \quad (17)$$

so

$$Z(x, y) = -\frac{2U^2}{g} \iint_R Y_\xi(\xi, \zeta) G_x(x - \xi, y, 0; \zeta) d\xi d\zeta. \quad (18)$$

Equation (18) gives the wave elevation directly, by an integration over the centre-plane, with input offset data $Y(x, z)$ and use of the assumed code for the Green's function $G(x, y, z; \zeta)$. The integration is of convolution type with respect to the x -variable, and the method could be called a convolution method.

It is possible to split G and hence the resulting wave elevation Z into various components as in the previous section. We shall write G^- to denote the corresponding function where the path of k -integration (incorrectly) goes below the pole, in order to distinguish it from the desired function G with the path above the pole. Then the difference $G^0 = G - G^-$ is again $-2\pi i$ times the residue, namely

$$G^0(x, y, z; \zeta) = -\frac{k_0}{\pi} \Re i \int_{-\pi/2}^{\pi/2} d\theta \sec^2 \theta e^{k_0 \sec^2 \theta [(z+\zeta) - i(x \cos \theta + y \sin \theta)]} \quad (19)$$

$$= -\frac{2k_0}{\pi} \int_0^{\pi/2} \sec^2 \theta e^{k_0(z+\zeta) \sec^2 \theta} \sin(k_0 x \sec \theta) \cos(k_0 y \sec^2 \theta \sin \theta) d\theta. \quad (20)$$

Similarly, we can define a Cauchy principal-value version of the Green's function, namely $G^C = (G + G^-)/2$. Note that G^0 is an odd function of x and G^C an even function of x , and $G = G^C + G^0/2$.

It is now simple to show that use of these special versions of the Green's function in the convolution (18) yields the same special wave elevations Z^0 and Z^C as in the previous section, e.g.

$$Z^0(x, y) = -\frac{2U^2}{g} \iint_R Y_\xi(\xi, \zeta) G_x^0(x - \xi, y, 0; \zeta) d\xi d\zeta. \quad (21)$$

Hence, if we choose, we can use convolutions such as (21) and the equivalent for Z^C to generate the full flow field $Z = Z^C + Z^0/2$.

However, the subdivision of the flow field into local and far-field contributions is not unique. We can define a local Green's function G^L analogous to (16), namely

$$G^L(x, y, z; \zeta) = G^C(x, y, z; \zeta) - \frac{1}{2} G^0(x, y, z; \zeta) \operatorname{sgn} x. \quad (22)$$

Note that this is an even function of x . However, if we then convolve with the body slope to generate a local wave field, namely

$$Z^L(x, y) = -\frac{2U^2}{g} \iint_R Y_\xi(\xi, \zeta) G_x^L(x - \xi, y, 0; \zeta) d\xi d\zeta \quad (23)$$

this is not the same as the local wave field Z^L defined in the previous section by equation (16), because of the influence of a factor $\operatorname{sgn}(x - \xi)$ from the second term of (22).

For example, the equivalent of (14) for the Green's function is

$$G = \begin{cases} G^L, & x < 0 \\ G^L + G^0, & x > 0 \end{cases} \quad (24)$$

or $G = G^L + G^0H(x)$. Hence if we use this in the convolution method, we have $Z = Z^L + Z^F$ where the local wave field Z^L is now defined by (23) rather than by (16). Similarly, the far-field wave is

$$Z^F(x, y) = -\frac{2U^2}{g} \iint_R Y_\xi(\xi, \zeta) G_x^0(x - \xi, y, 0; \zeta) H(x - \xi) d\xi d\zeta \quad (25)$$

which is not in general the same as the quantity $Z^F = Z^0H(x)$ defined in (15). Incidentally (with the origin located between bow and stern) there is a difference between the two forms of the local field only when x lies between that for the bow and stern; ahead of the bow both Z^F are exactly zero, and aft of the stern they are both equal to Z^0 . In any case, both methods must end up with the same total field $Z = Z^L + Z^F$ everywhere.

4 Damping due to eddy viscosity

It is possible to include viscosity in the far-field calculations by introducing to the integrands of the integrals (11) and (20) the multiplicative factor

$$\exp(-2\nu k_0^2 \frac{x}{U} \sec^4 \theta) \quad (26)$$

where ν is the eddy viscosity. At each fixed angle θ of propagation, this factor is as estimated by Lamb ([4] p. 625) for damping of plane waves. Lamb's derivation is for laminar flow with ν as the (molecular) kinematic viscosity, which is of the order of $10^{-6}\text{m}^2\text{s}^{-1}$. However, we use it here in a turbulent context with a much larger value of ν , corresponding to an eddy viscosity. The actual value of ν is not precisely known in any given situation, and indeed is not necessarily a constant in space, varying over a wide range of values. Use of any prescribed constant value for an eddy viscosity is just an empirical first step toward a more accurate model of turbulent flow. Nevertheless, oceanographically relevant ([6] pp. 9, 413, [1] pp. 45, 63, 72) values of eddy viscosity seem to be of the order of 10^{-3} to $10^{-2}\text{m}^2\text{s}^{-1}$, and here we take $\nu = 0.005\text{m}^2\text{s}^{-1}$ as representative.

Such an eddy viscosity primarily damps out those waves that oscillate most rapidly, and the present damping factor can be seen from its form (26) to act most

strongly on those waves for which θ is near $\pm\pi/2$; that is, the short divergent waves travelling nearly perpendicular to the track of the ship. It is believed that eddy viscosity has little effect on the local field, and we make no attempt to include it in that component here.

5 Domains of computation

The enhancement to be made to SWPE in this version SWPE3.0 is to evaluate the local-field component Z^L as the complement to the already-available SWPE2.0 far-field calculation of Z^F .

The nature of the local field is that it does not have waves ahead of the bow nor aft of the stern, but simply represents the disturbance to the surface due to changes in the dynamic pressure as the surrounding fluid is accelerated by the body. As such, it can be expected to decay monotonically towards zero as the distance from the ship increases toward infinity. This monotonic behaviour can be utilised to computational advantage.

In either of the two formulations described above, evaluation of the local-field component requires computation of a double integral with respect to θ and k . The new k -integration can be performed as a Cauchy principal-value, either in equation (10) for the Michell P, Q formulation, or in equation (1) for the Green's function itself in the convolution formulation. The far field, by comparison, involves only the residue from the k -integrand, and is a single integral with respect to θ . Of course, both integrals must then be further integrated over the body, so in reality there are quadruple and triple integrals respectively which must be evaluated for each field point being considered. As a result, it is the local-field computation which one might expect to be the most expensive in the evaluation of the total wave field.

However, Newman [8] observed that, in the convolution formulation, one need only evaluate this double integral for the Green's function, namely G^L as defined in (22), once *ever* (but for every possible value of $x - \xi$, y and $z + \zeta$). Furthermore, since G^L is waveless and, in particular, tends monotonically towards zero at infinity, it is possible to accurately approximate the local Green's function by a polynomial. Thus, as a *separate* task, one can determine G^L , and then determine coefficients for reconstruction of values of this function by a polynomial. This task was performed by Newman, and details of the method, algorithms for the associated code, and values for the polynomial coefficients are all given in [8].

The resulting computational savings are significant, since the double integra-

tion is replaced by summation of finite series, which is comparable in terms of computational effort with the single integration required for the far-field calculation. There is, however, a small price to be paid when moving on to compute the total field. The local-field component evaluated in the above manner is that of the convolution formulation as defined in equation (23), and therefore is the complement to the convolution far field (25). However, this is *not* in general the far field (11) determined by SWPE2.0. However, as already noted, both far-field formulations are equivalent beyond bow and stern, and thus the local-field component can be used to complement the far field of SWPE2.0 everywhere except between bow and stern. Between bow and stern it is necessary to use equation (25) to determine the far-field component.

One may ask, “Why not use the far field of the convolution formulation everywhere?” Indeed this would be entirely acceptable, except that one of the advantages of the previous version SWPE2.0 is then lost. SWPE2.0’s unique Michell P, Q formulation allowed significant increases in computation speed which are not available with the far field of the convolution formulation, and so such an approach would be slower. Thus, for optimum speed of computation, we use two domains of computation. The first is between bow and stern, and the second is elsewhere. Between bow and stern, the slower far-field convolution integral (25) is added to the local field as computed using the Newman polynomial representation. Elsewhere, the far field as computed by the Michell P, Q code in SWPE2.0 (11) is added to the (same) local field.

A further optimisation is possible by considering a third domain in which the local-field correction is sufficiently small as to be neglected entirely. In this domain the program would revert to being exactly the same as SWPE2.0. However, as the resulting increase in speed is minimal, this optimisation is not included in the present version of SWPE.

5.1 Accuracy and timings

Even though, as discussed above, there are computation methods which are inefficient relative to the final choices built into SWPE, some of these were also programmed to use as benchmark checks on the accuracy of the main code. This check was in all cases satisfactory, i.e. it was always possible to increase accuracy-determining input parameters such as the number of intervals into which integration ranges were divided, until there was agreement to at least 3 significant figures between the various computation methods.

The following are sample computation times per wave elevation point on a

SUN Sparc Ultra (averaged over many such points), at approximately 3-figure accuracy. Some runs were made on other machines, both slower and faster. For example, timings when the program was run on one CPU of a Silicon Graphics Power Challenge were found to be about 4 times faster.

A direct numerical double integration of (10) took 260 seconds per point, which would be quite prohibitive if the intention was to use SWPE to survey many thousands of points. A compromise method where the k -integration of (1) was done by a polynomial representation (as a complex exponential integral) but the θ -integration done numerically took 18 seconds per point.

Use of the full Newman [8] polynomial representation for the double integral then cut this time to 5 seconds for the total flow field when the convolution method was being used for the single integral, but nearly all of this computer time was occupied in evaluating that single integral. This is the method that is used (of necessity) in SWPE between bow and stern. Finally, if we use the (more efficient) Michell method for the single integral combined with the Newman method for the double integral, which SWPE uses for points not between bow and stern, the time was further dramatically reduced to about 0.25 seconds, of which almost all was for the double integral part.

A 100MHz Pentium PC with 16Mb of RAM was found to be approximately 4 times slower, while both a 450MHz Pentium PC with 256Mb RAM and a Silicon Graphics Power Challenge were found to be about 4 times faster. However, the test used only one CPU of the twenty available for the Power Challenge, and a further increase in speed by a factor of nearly 20 may be expected if the machine was dedicated to the task.

Various input parameters affect accuracy, and appropriate values are specified in the SWPE3.0 User's Manual [15]. One of the most important is the number N_θ of θ values into which the basic range $(0, \pi/2)$ is divided in carrying out the θ -integration numerically. We have found that for surface vessels, especially in the absence of eddy viscosity, values of N_θ of at least 640 are needed, and values of 1280 or more are recommended. If N_θ is too low, some of the diverging waves that are very noticeable at the inside edge of the Kelvin angle are missed. Of course, if the body is submerged or if an eddy viscosity correction factor is being used, these diverging waves near to $\theta = \pi/2$ are damped out, and this is then not such a critical matter.

The other set of inputs that affect accuracy are the offset data specifying the ship. Again, there are parts of the computation where it is necessary to specify the hull geometry more accurately than is common in naval architectural practice. In particular, for the DTMB 5415 model, the number of waterlines is critical. We



Figure 1: David Taylor Model Basin hull 5415.

have found differences of the order of one or two percent between results with 23 waterlines and 89 waterlines. The latter seems rather extreme, but it should be noted that because this vessel has a bow bulb that extends beneath its main keel, many of these waterlines are “wasted”, with zero input offsets, and it is necessary to use a large number of waterlines simply to define adequately the shape of the bulb and the transom. For more conventional vessels, a smaller number of offsets may be acceptable. The number of stations is less sensitive, but we recommend at least 51 stations to maintain 3-figure accuracy.

6 Comparison with the Wake-Off

To compare our predictions of wave elevations with experimental results, we use the DTMB 5415 hull shown in Figure 1 (see [2]), which is representative of a modern destroyer. This hull has a shallow transom stern and is also equipped with a large sonar dome situated beneath the bow stem.

The 5415 hull was used in the “Wake-Off” study of Lindenmuth et al [5] wherein predictions by several computer codes were compared with experimental results obtained in a towing tank on a model of length 5.72 metres. Hull offsets, experimental results and other data are available in electronic form at the DTMB WWW site [2].

Experimental results are available for two Froude numbers, namely $F = 0.2755$ and $F = 0.4136$, which correspond to model speeds of 4 and 6 knots and full scale speeds of 20 and 30 knots respectively. Hull 5415 offsets, supplied in `Plot3d` format by the DTMB WWW site, were converted to `TX4` panelised format by a simple FORTRAN program. The `TX4` format offsets were then converted to `SWPE` format (which requires uniformly spaced stations and waterlines) using a special data-conversion program `two_d_projector` [12]. Two `SWPE` input files were prepared, one for each Froude number. The offsets and hull dimensions in each file are for the hull in the squatted attitude appropriate to each Froude num-

ber. These input files have been included with the SWPE3.0 distribution files, as has the data-conversion program `two_d_projector`.

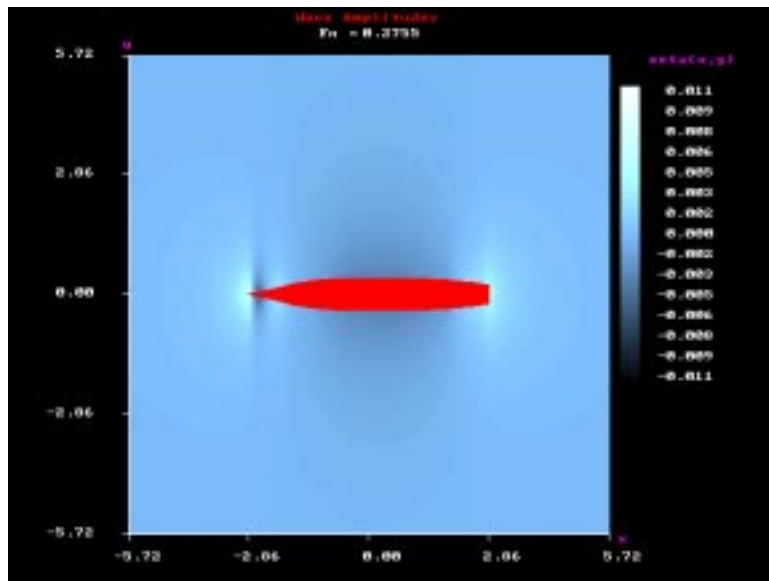
6.1 Comparison of wave-field components

Figure 2 shows a surface image of the local-field contribution, accompanied by a wave cut along $y = 0.572\text{m}$ displaying both the local-field component and the total wave elevation as determined by SWPE for the 5415 hull at a Froude number of 0.2755. Figure 3 shows the same information, but for a Froude number of 0.4136. The wave cut is offset from the centreplane by one-tenth the ship's length, and so lies near to the side of the ship, whose half-beam is 0.4m. One can see that the local-field component decays monotonically to zero as $r \rightarrow \infty$ from bow and stern, whereas the total wave elevation, and hence the far-field component, is wave-like behind the ship. As mentioned earlier, the local field disturbance can be considered to be due to the change in dynamic pressure of the fluid as particles are accelerated by the ship. The far field is due to the oscillatory motion set up by the restoring force of gravity. Of most interest is the fact that the local field is of negligible amplitude relative to the far-field component for distances greater than one shiplength behind the ship. For example, for $F = 0.4136$ at $x = 5.72\text{m}$, half a shiplength behind the stern, the amplitude of the local-field disturbance is 0.0006m, which is less than 1% of the amplitude of the total far-field disturbance along the wave cut. It is this extremely rapid decay of the local field that makes the previous version SWPE2.0 of the present code valid for most of the region of interest.

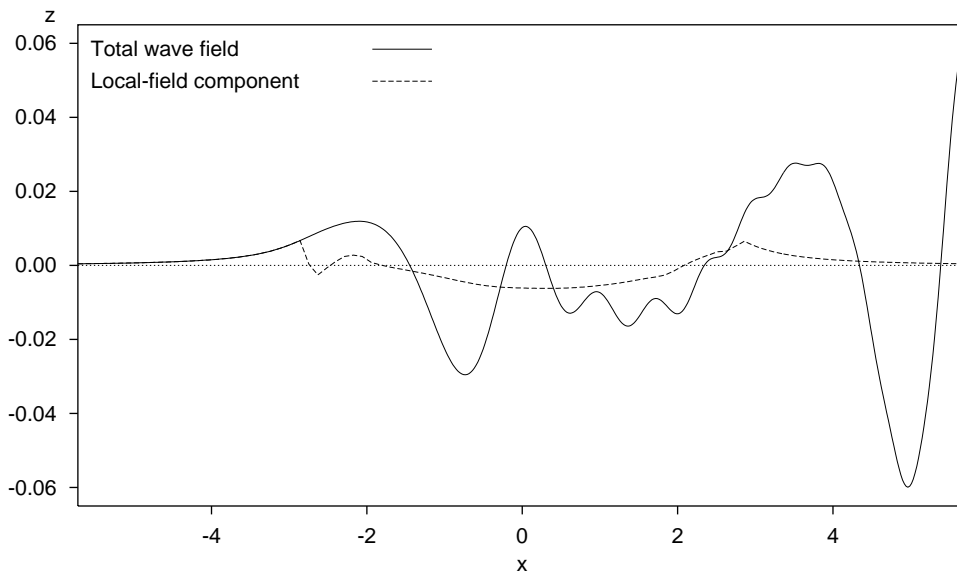
6.2 Effect of eddy viscosity

As described in Section 4, it is possible to introduce a damping factor into the formulation to represent effects of eddy viscosity. Figure 4 shows the effect of eddy viscosity on free-surface elevations along the wave cut $y = -1.854\text{m}$ for the 5415 hull at Froude number 0.2755, for values of eddy viscosity ranging from $\nu = 10^{-4}$ to $\nu = 10^{-2}\text{m}^2\text{s}^{-1}$, along with the corresponding inviscid case $\nu = 0$. Similarly, Figure 5 shows this effect at $F = 0.4136$. One can see that viscous damping has the greatest effect on the diverging waves, and at the larger viscosities the only remaining disturbance is due to the transverse wave system.

The smaller values of viscosity simply remove some very short diverging components, so smoothing out the main transverse crests and troughs, without essentially reducing their amplitude. There is little difference between the curves for

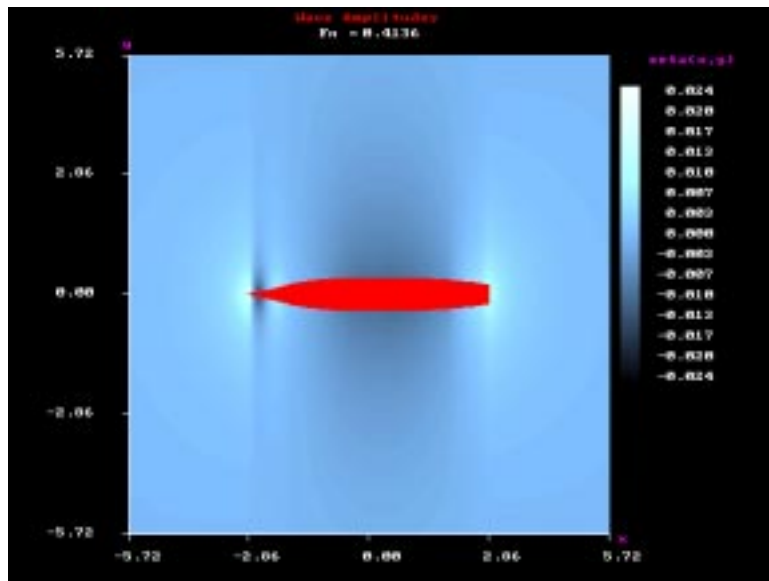


(a)

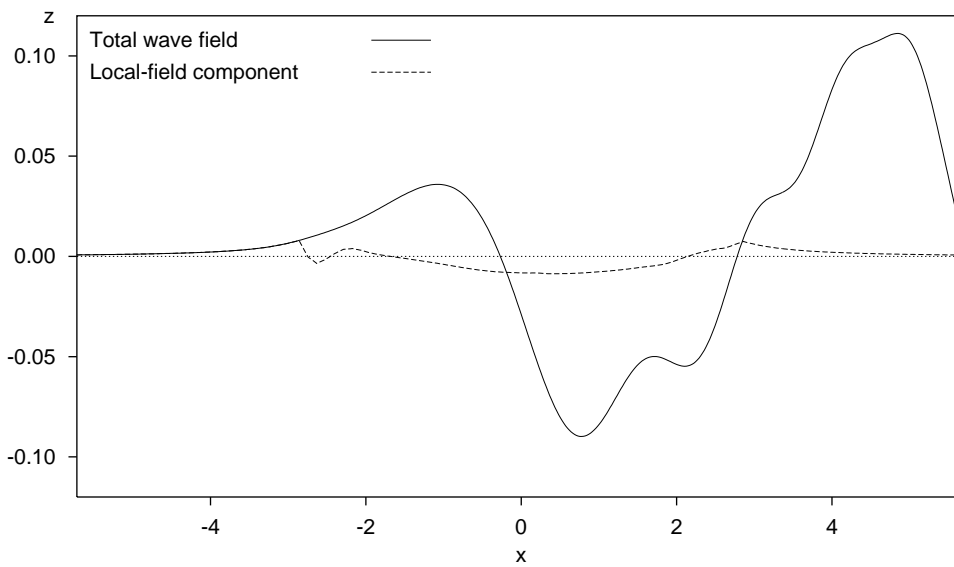


(b)

Figure 2: (a) Surface image of the local-field contribution and (b) comparison of total wave elevations and local-field contribution along the wave cut $y = 0.572\text{m}$ produced by SWPE for the 5415 hull at Froude number 0.2755.



(a)



(b)

Figure 3: (a) Surface image of the local-field contribution and (b) comparison of total wave elevations and local-field contribution along the wave cut $y = 0.572\text{m}$ produced by SWPE for the 5415 hull at Froude number 0.4136.

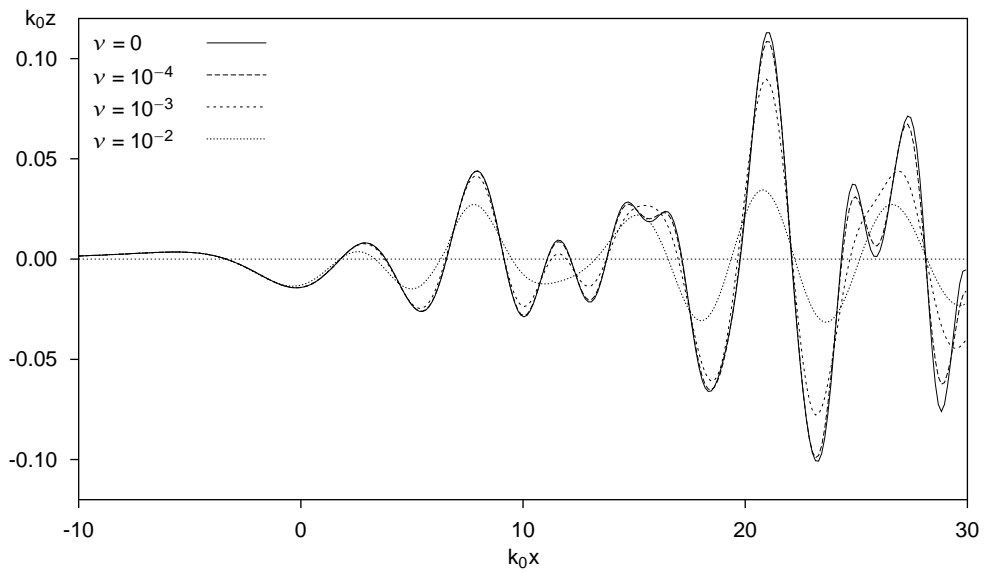


Figure 4: Effect of eddy viscosity on wave elevations at $y = -1.854\text{m}$ from the ship's track produced by SWPE for the 5415 hull at Froude number 0.2755.

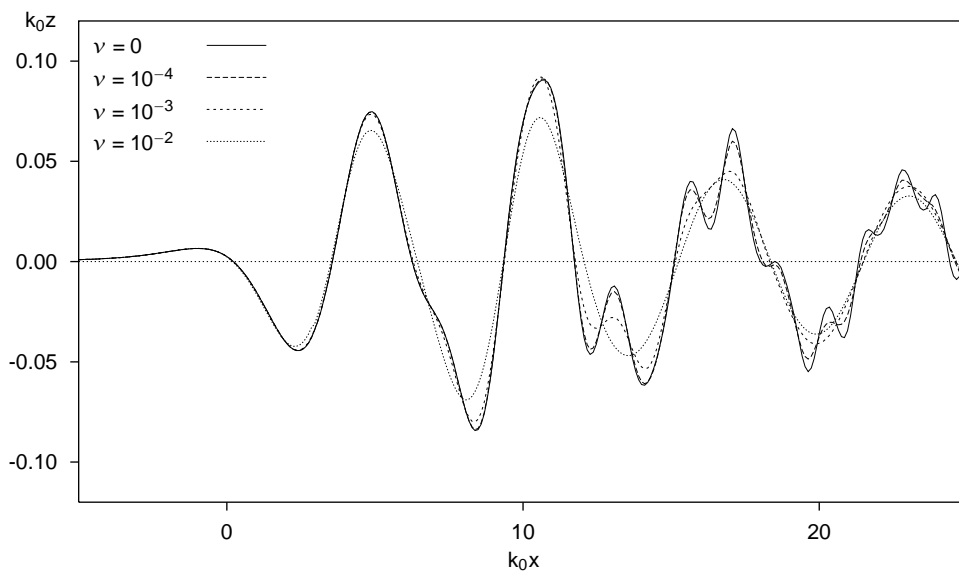


Figure 5: As for Figure 4, but with Froude number 0.4136.

eddy viscosity equal to zero and $0.0001\text{m}^2\text{s}^{-1}$, at both Froude numbers. On the other hand, the larger values of viscosity reduce the transverse wave amplitudes, to the extent that waves decay with distance behind the ship faster than is observed in practice. In fact, the decay rate observed in the model experiments is also somewhat higher than one might expect, a fact that was commented upon in [5], and this feature may not be real. Nevertheless, at realistic intermediate values of the order of $0.005\text{m}^2\text{s}^{-1}$, the agreement with experiment is significantly enhanced by use of this eddy viscosity correction factor.

6.3 Transom stern condition

The 5415 hull has only a small transom, even when the hull is trimmed and squatted. We should therefore expect only small differences between predictions assuming that the transom is running fully dry (that is, a functioning transom with non-zero stern offsets from which the flow separates to form a wake) and when it is completely wet (a state where there is in effect no transom, the offsets returning suddenly to zero at the stern and the flow being assumed to follow this sharp corner). This is supported by Figures 6 and 7 which show that there are only slight differences between the two transom conditions. For $F = 0.4136$, the largest difference occurs at the second peak near $k_0x = 11.0$.

6.4 Comparison with competitors

The following two figures, 8 and 9, show the prediction of the wave elevations as determined by SWPE along with those predicted by competitors in the Wake-Off. Also included are the actual experimental results. It is interesting to note that there is in general better agreement between the various numerical predictions than there is with the experimental result. In addition, the experimental results display some characteristics which are surprising (such as a negative mean elevation and a large rate of decay in amplitude), that perhaps give some reason to doubt their accuracy. At the very least, it is clear that SWPE is producing results as good as any of the Wake-Off competitors, and significantly better than most. The best of the competitors is the program “FARWAV” of Noblesse [9] and our code is quite close in spirit and in its output to that program, the theoretical basis for which has also been extended since 1991, see e.g. [10].

Subsequent to the 1991 Wake-Off, there have been a few additional computations for the same DTMB 5415 hull. Notable is the commercial code “RAPID” of MARIN, due to Raven [11], which is fully nonlinear. Figure 10 shows the

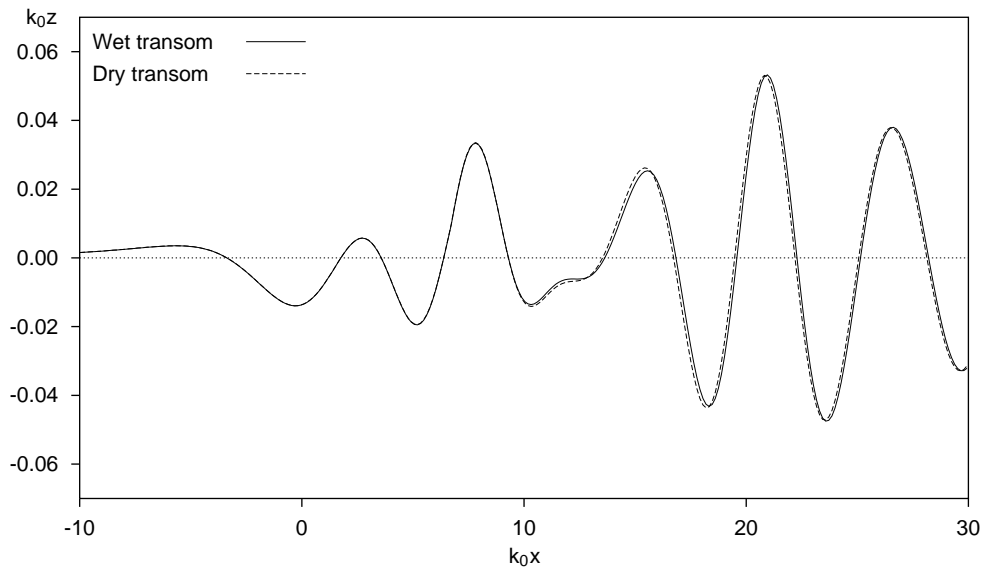


Figure 6: Comparison of wave elevations produced by the dry and wet transom conditions at $y = -1.854\text{m}$ from the ship's track produced by SWPE using an eddy viscosity of $0.005\text{m}^2\text{s}^{-1}$ for the 5415 hull at Froude number 0.2755.

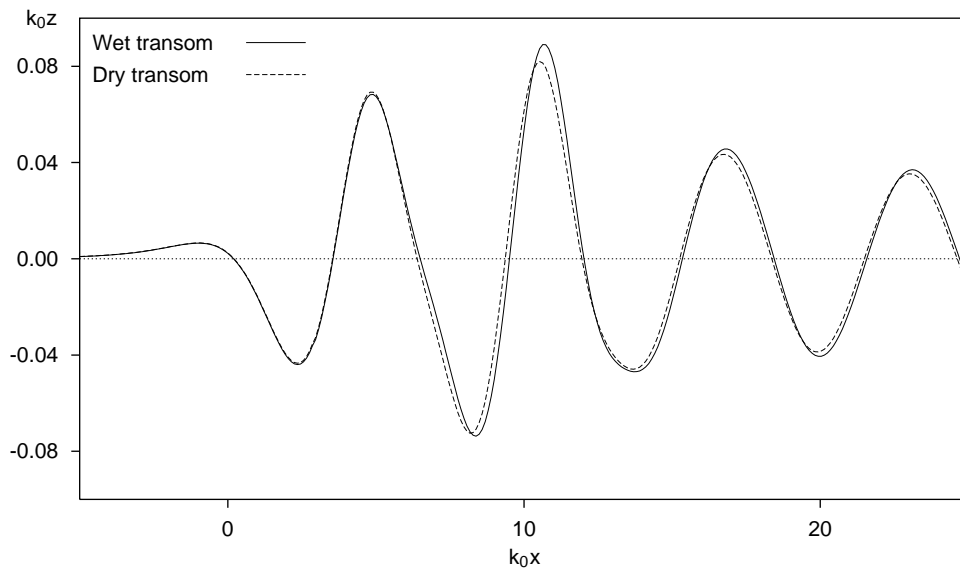


Figure 7: As for Figure 6, but with Froude number 0.4136.

RAPID, SWPE, and experimental results at $F = 0.4316$. Again, our results are comparable in accuracy with those produced by RAPID. This is indirect evidence that nonlinearity is not particularly important, and the Michell thin-ship approximation is adequate for ships of this slenderness. More direct evidence of validity of the thin-ship approximation for submerged bodies was already provided in the second SWPE report [14].

We conclude by displaying two figures, 11 and 12, showing wakes determined by SWPE for the 5415 hull at Froude numbers 0.2755 and 0.4136 respectively. These two figures both show the wave field only out to $x = 13\text{m}$; the cover of this report shows a larger view (to $x = 25\text{m}$) of the same waves at Froude number 0.4136. These computations were performed with eddy viscosity $0.0001\text{m}^2\text{s}^{-1}$, which is lower than our recommended value, so that the very fine diverging wave structure is visible, especially at the inside edge of the main “bow wave” at the Kelvin angle of 19.5° . Larger values of eddy viscosity eliminate some of this structure, and it is an open question at this time as to whether this improves or degrades agreement with observation. What is clear however, is that this structure is real in the absence of eddy viscosity, and can be missed if less-accurate numerical algorithms are adopted.

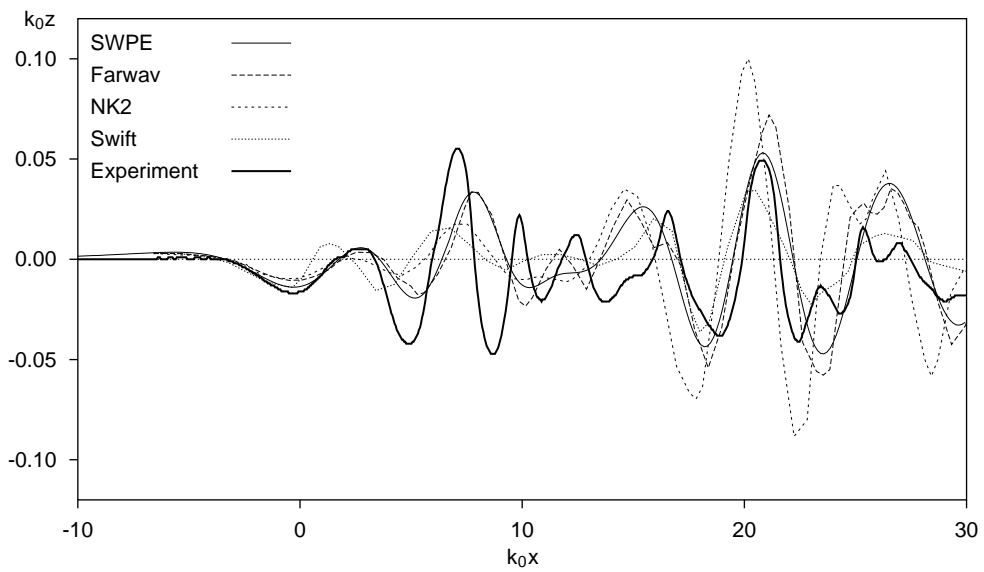


Figure 8: Comparison of wave elevations at $y = -1.854\text{m}$ from the ship's track produced by SWPE (using an eddy viscosity of $0.005\text{m}^2\text{s}^{-1}$) and estimates made by several competitors in the Wake-Off for the 5415 hull at Froude number 0.2755.

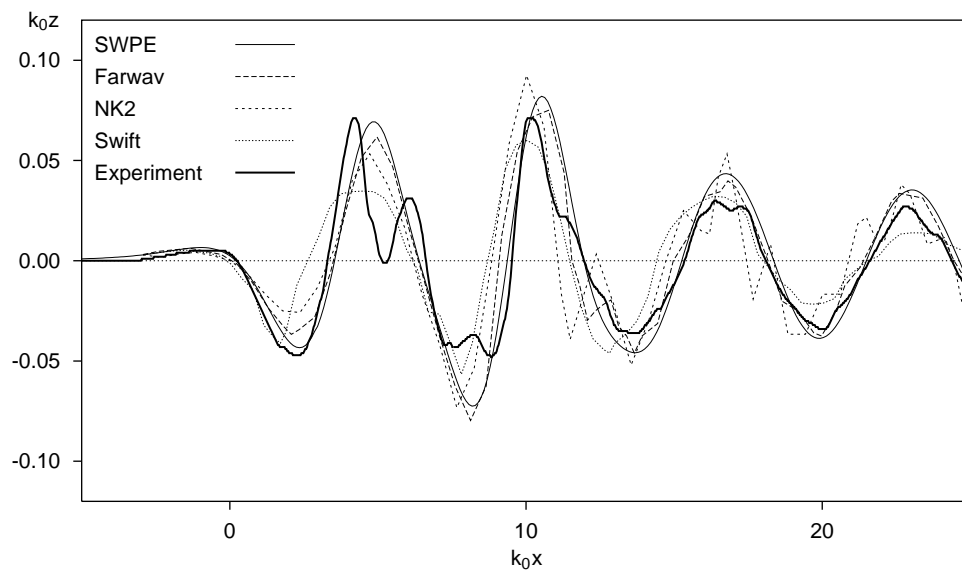


Figure 9: As for Figure 8, but with Froude number 0.4136.

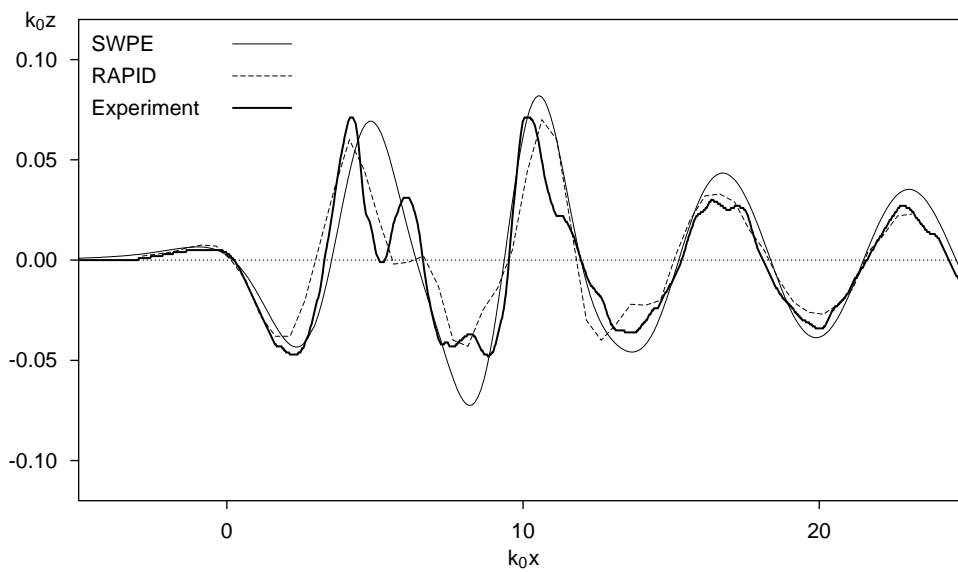


Figure 10: Comparison of wave elevations at $y = -1.854\text{m}$ from the ship's track produced by SWPE (using an eddy viscosity of $0.005\text{m}^2\text{s}^{-1}$) and estimates made by the MARIN code "RAPID" [11] for the 5415 hull at Froude number 0.4136.

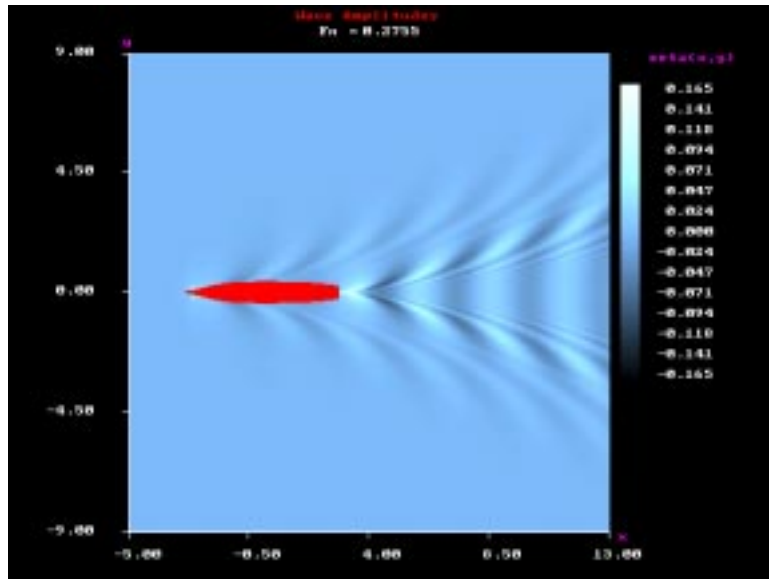


Figure 11: Wake as determined by SWPE for the 5415 hull at Froude number 0.2755.

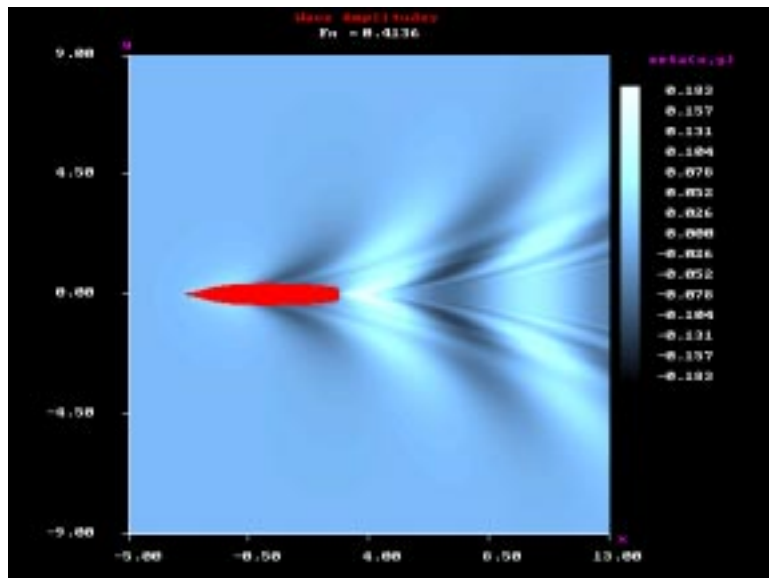


Figure 12: Wake as determined by SWPE for the 5415 hull at Froude number 0.4136.

References

- [1] Cushman-Roisin, B. *Introduction to Geophysical Fluid Dynamics*. Prentice-Hall, Englewood Cliffs, NJ, 1994.
- [2] David Taylor Research Center, <http://www50.dt.navy.mil/5415>, 1995.
- [3] Havelock, T.H. *Wave resistance*. Proc. Roy. Soc. Lond. Ser. A. **118** (1928) 24–33.
- [4] Lamb, H. *Hydrodynamics*. 5th Edn., Cambridge 1932.
- [5] Lindenmuth, W.T., Ratcliffe, T.J., and Reed, A.M. *Comparative accuracy of numerical Kelvin wake code predictions – “Wake-Off”*. David Taylor Research Center Report DTRC-91/004, Department of The Navy, Bethesda, MD, USA, 1991.
- [6] Mei, C.C. *The Applied Dynamics of Ocean Surface Waves*. Wiley, New York 1983.
- [7] Michell, J.H. *The wave resistance of a ship*. Phil. Mag. (5) **45** 106–123 (1898).
- [8] Newman, J.N. *Evaluation of the wave-resistance Green function: Part 1 — The double integral*. J. Ship Res. **31** 79–90 (1987).
- [9] Noblesse, F. *A slender ship theory of wave resistance*. J. Ship Res. **27** 1983.
- [10] Noblesse, F., Yang, C., Lohner, R. and Hendrix, D. *Fourier-Kochin representation of far-field steady ship waves*. 7th Journées de l’Hydrodynamique, Marseille, March 1999.
- [11] Raven, H.C., *A solution method for the nonlinear ship wave resistance problem*. Doctoral Thesis, Technical University Delft, 1996.
- [12] Scullen, D.C., *two_d_projector*, A FORTRAN program to convert TX4 panelised hull data to constant-spacing form, 1999.
- [13] Tuck, E.O., Lazauskas, L. and Scullen, D.C., *Sea Wave Pattern Evaluation, Part 1 report: Primary code and test results (surface vessels)*, Department of Applied Mathematics, The University of Adelaide, April 1999.

- [14] Tuck, E.O., Scullen, D.C. and Lazauskas, L., *Sea Wave Pattern Evaluation, Part 2 report: Investigation of accuracy*, Department of Applied Mathematics, The University of Adelaide, May 1999.
- [15] Tuck, E.O., Lazauskas, L., and Scullen, D.C., *Sea Wave Pattern Evaluation, SWPE3.0 User's Manual*, January 2000.
- [16] Tuck, E.O. *A submerged body with zero wave resistance*. J. Ship Res. **33** (1989) 81–83.
- [17] Wehausen, J.H. and Laitone, E.H., *Surface Waves*, in Handbuch der Physik, ed. Flugge W., Ch. 9. Springer-Verlag, 1962.